Earth's Cryosphere, 2021, vol. XXV, No. 5, pp. 47–59 http://earthcryosphere.ru/

GROUND-PENETRATING RADAR SOUNDING OF DEPOSITS WITHIN THE LIMITS OF HIGH-CENTERED POLYGONS IN THE ARCTIC

D.E. Edemskiy[1], V.E. Tumskoy[2], A.N. Ovsyuchenko[3]

[1] *Pushkov Institute of Terrestrial Magnetism, Ionosphere and Radio Wave Propagation, RAS, 4 Kaluzhskoe hwy, Troitsk, Moscow, 108840, Russia; deedemsky@gmail.com*

[2] *Melnikov Permafrost Institute, SB RAS, Merzlotnaya str. 36, Yakutsk, 677010, Russia*

[3] *Schmidt Institute of Physics of the Earth, RAS, B. Gruzinskaya str. 10, bld. 1, Moscow, 123242, Russia*

This article analyses the results of *Loza-V* georadar sounding of the upper part of the permanently frozen ground section in the area of polygonal patterns development. These investigations took place on the eastern coast of the Taymyr Peninsula and on the western coast of Kotelny Island (New Siberian Islands). The polygonal pattern is at the descend stage of development at both sites, so the ground-penetration radar profiles were scanned across the flat and high-centered central parts of the polygons. The results allowed us to determine some peculiarities of ground-penetrating radar profiles for polygons with different types of surfaces, composed mainly of sand-gravel deposits. Typical ground-penetrating radar complexes corresponding to the central parts of the polygons and deposits overlapping thawed ice wedges were identified. The possibility of using the spectrum of waveforms to interpret results was shown, velocities of electromagnetic wave propagation in the studied deposits were determined. Ice wedges and pseudomorphs after them were not reliably identified, but areas of their possible location were.

Keywords: *ground-penetration radar, polygonal pattern, spectrum of waveforms, hodograph diagram, Taymyr Peninsula, Kotelny Island.*

INTRODUCTION

In the area of the development of permafrost (the cryolithozone) polygonal forms of microrelief are widely distributed. They are known from the steppes of Zabaikalye in the south to the arctic deserts in the north, being most widely represented in zones from the forest tundra to arctic deserts. In the middle of the 20th century, it was already known that the reason for the formation of a polygonal patterned ground is the process of frost cracking [*Dostovalov, 1952; Romanovskii, 1977*]. As a result of temperature tensions during winter season narrow vertical cracks form in the top horizons of permafrost. Depending on environmental conditions they can fill with silty and sandy material, leading to the formation of primary-sand or sand-ice wedges, and in more humid conditions the cracks fill with snow meltwater and, with time, ice wedges are formed. During the long-term ice wedge growth, the ground rims, or ramparts, form on the surface of the earth above them. On the surface the ramparts above the ice wedges form a polygonal, most often a tetragonal, network. Water accumulates between the ramparts, and shallow center ponds form (Fig. 1, *a*). The ramparts vary from 0.1 to 0.5 m in height, the depth of the ponds usually constitutes 0.5–1.0 m. The diameter of the polygons changes from 3–5 to 100–150 m, usually within a range of 10–25 m.

When the active layer thickness increases as a result of grow of the mean annual ground surface temperature, the thawing of the top parts of the ice wedges begins, so that the polygonal surface evens out and becomes almost smooth. Upon further thawing, troughs form above the ice wedges, as a result of which the initial low-centered ice-wedge polygons transform into a polygonal flat-centered (intermediate-centered) peatland with troughs above *ice* wedges, so the topography becomes inverse (Fig. 1, *b*). If ice wedge-containing deposits thaw more slowly but have a high ice content, cone-like mounds (thermokarst mounds, or baidzharakhs) with a height of 2–4 m appear between the thawing wedges (Fig. 1, *c*). As a result of total thawing of ice wedges, wedge-shaped or concaved thaw structures called pseudomorphs remain in their place in the outcrop around the perimeter of the polygons [*Kaplina, Romanovskii, 1960*].

The main features of a polygonal pattern are the polygons' configuration on the surface, their diameter, defined as the distance between the axes of parallel ice wedges, and the width of ice wedges. The solution of many scientific and practical problems requires knowledge of the composition of deposits and the peculiarities of the inner structure of the central parts of the polygons, which are usually called ground columns. These features can by far not always be quickly obtained using geological methods, so the more effective utilization of geophysical methods is of significant interest.

The ground-penetrating radar sounding method can be used to determine some features of a polygonal network (the peculiarities of its inner structure, the width of its ice wedges, the diameter of its polygons) and to more specifically define its areal distribution. The fields of application of GPR sounding are wide: geology, construction, archaeology, ecology, etc. [*Finkelstein et al., 1986; Vladov, Starovoytov, 2004; Buzin*

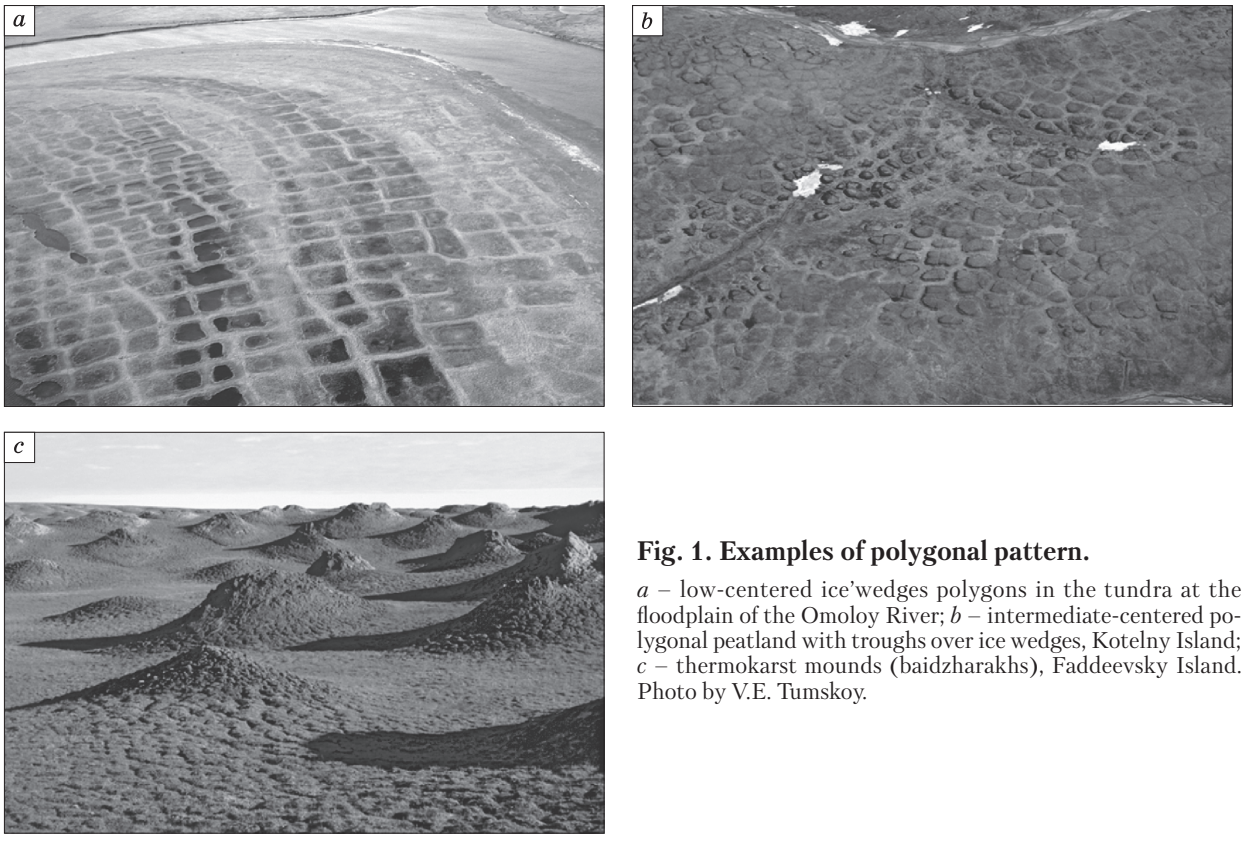

Fig. 1. Examples of polygonal pattern.

a – low-centered ice'wedges polygons in the tundra at the floodplain of the Omoloy River; *b* – intermediate-centered polygonal peatland with troughs over ice wedges, Kotelny Island; *c* – thermokarst mounds (baidzharakhs), Faddeevsky Island. Photo by V.E. Tumskoy.

et al., 2017; Edemskiy et al., 2019]. In permafrost zone it is also widely used for the solution of geological-geophysical and engineering problems, as well as soil research [*Voronin, 2015; Léger et al., 2017; Sudakova et al., 2017*].

The article presents some results of studies of the structure of ground columns under the polygonal flat-centered peat mounds in the Arctic, which were obtained during the Complex Expedition of the Northern Fleet with the participation of the Russian Geographical Society "Franz Josef Land Archipelago – 2020" in August–October 2020.

EQUIPMENT AND METHODS OF FIELD WORK

The high-power *Loza-V* GPR [*Kopeikin et al., 1996; OOO "VNIISMI", 2021*], which has been used to solve various practical problems over the course of the past 10 years [*Kopeikin et al., 2012; Voronin, 2015; Edemskiy et al., 2018, 2019*], was used in this field research. As a result, tremendous positive experience both in conducting field work and in GPR data processing and interpretation techniques has been acquired.

The *Loza-V* GPR included transceiver antennas with a center frequency of 100 MHz (A100) and 150 MHz (A150), which provided an opportunity to sound at a depth interval from several dozens of centimeters to 10–15 m, depending on the electromagnetic properties of the medium. GPR sounding was completed by the profile, with location registration at each scanning point, for which a Garmin CX60 GPS receiver was used.

To achieve correct interpretation of the obtained GPR profiles and for the reconstruction of the geological section based on these profiles the sounding was performed based on the common depth point (CDP) method with a subsequent (0.1 m interval) increase of the distance between the "transmitter – receiver" antennas from 0.2 m to 6 m [*Vladov, Starovoytov, 2004; Edemskiy et al., 2010*]. This method allows for determining electromagnetic wave velocity in each layer of the GPR section and transforming the section from a scale of time to a scale of depth without using *a priori* information.

Standard processing modes were used to process data: appropriate values of increasing signal strength, brightness and contrast were chosen, bandpass filtering of signals and averaging functions were applied. On the final stage of processing and analysis a digital elevation model of the area was superimposed on the GPR profile.

Spectral analysis of GPR sounding results was applied during source data analysis. In accordance

with the theory of wave distribution [*Finkelstein, 1986; Vladov, Starovoytov, 2004*], the spectrum of the temporal signal form presents as a derivative of the spectrum of the source sounding signal and frequency characteristic of the media:

$$S(\omega) = S_0(\omega) \cdot K(\omega),$$

where $S(\omega)$ is the spectrum of the temporal signal form, $S_0(\omega)$ is the spectrum of the sounding signal, and $K(\omega)$ is the frequency characteristic of the media which presents as a characteristic of a filter of low frequencies, the parameters of which are determined by the properties of the media and are related to the structure of the section, the presence and properties of various reflecting boundaries and objects. Lately, the temporal spectral analysis was used to solve problems such as determining the percentage content of clay, mapping the soil moisture distribution, determining the boundaries of geological layers, ground ice conditions in permafrost, etc. [*Benedetto, Tosti, 2013; Anbazhagan et al., 2014; YongShuai et al., 2019; Neradovskii, Fedorova, 2020*].

Because of a significant difference between the velocity of electromagnetic wave propagation in different layers of the GPR section and changing depths of layer boundary location along the profile, understanding GPR profile depth in terms of meters is very difficult. All GPR profiles are presented using axes: x – profile step, in meters, y – double wave travel time, in nanoseconds.

To interpret the obtained data we used descriptions of surface topography at research points and shallow (no deeper than 0.5 m) trial pits within the active layer for describing deposit composition.

RESULTS OF GROUND-PENETRATING RADAR SOUNDING OF DEPOSITS

GPR sounding of the central parts of polygons was conducted in two areas (Fig. 2). The first one is located on the western coast of Maria Pronchishcheva Bay at eastern Taymyr, the second one – on the sea coast southwest of Nerpalakh Laguna (Kotelny Island, New Siberian Islands archipelago). Quite severe permafrost conditions with a mean annual ground temperature of about –11 °C and ongoing thermal contraction cracking even in coarse grain deposits is typical for these areas. The thickness of the active layer rarely exceeds 0.5 m.

Maria Pronchishcheva Bay, eastern Taymyr

Maria Pronchishcheva Bay is located on the eastern coast of Taymyr Peninsula and is approximately 50 km long. From the southwest the bay is limited by the spurs of the Byrranga Mountains divided by river valleys. The rivers exit at foothill plain 0.5–2.5 km wide, forming a series of terraces. At the mountain edge where a young tectonic scarp and a series of low (up to 30 m) young anticline ridges stretch, the terraces decline to the level of the floodplain. From the west, the scarp and ridges limit the coastal lowland with numerous lagoons which fully flood during wind surges up to 1.5–2.0 m high. The study area was located near the mouth of the Yuzhnaya River (Fig. 3, *a*), the coordinates of the area are 75°38′33.61″ N, 112°49′25.76″ E.

The near-surface part of the section is composed of marine (alluvial-marine?) deposits, the thickness of which increases towards the coast of the bay from

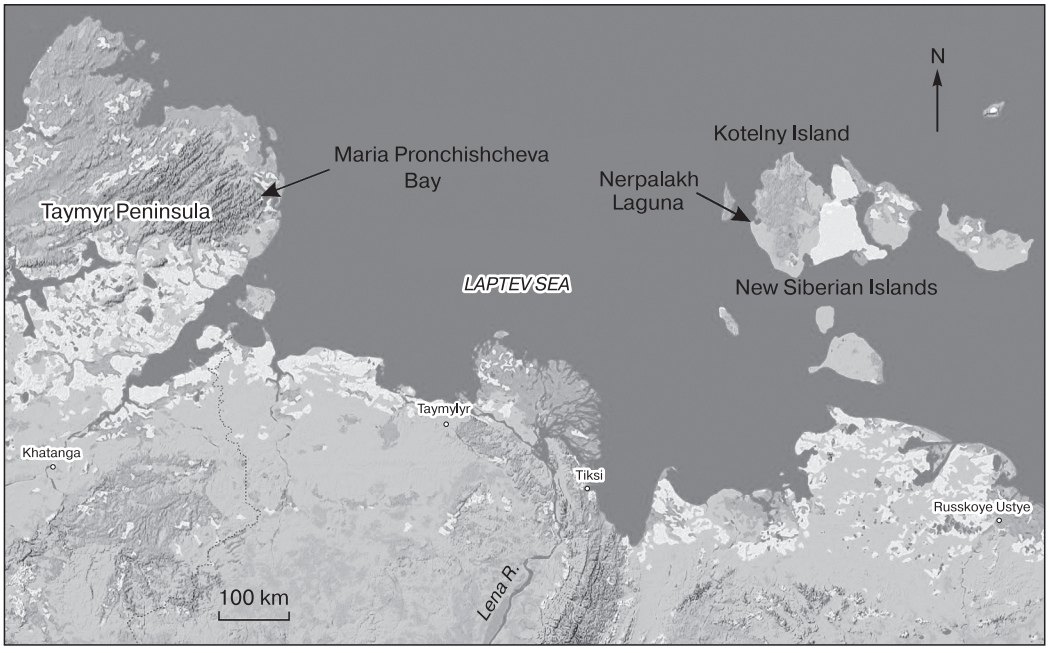

Fig. 2. Location of work sites.

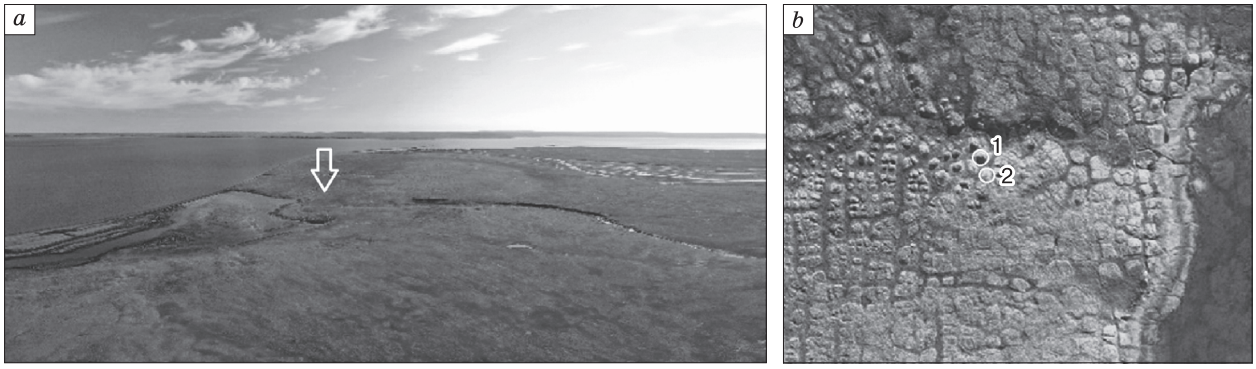

Fig. 3. Study site on the western coast of M. Pronchishcheva Bay.

a – general view of the bay coast (the arrow shows the position of sounding site); *b* – studied polygons (1 – high-centered, 2 – flat-centered). Photo by R.A. Zhostkov.

3 to 6–8 m. The deposits present as gravel-pebble material with interlayers of fine-grained sands and organogenic silts, the section of which is exposed in the bank outcrop of the stream. A peat layer covers the sand-gravel deposits, it's thickness varies from 0.3 m to 0.5 m in its eastern part, where GPR sounding was completed.

A polygonal patterned ground, represented predominantly by flat polygons divided by troughs above the ice wedges, is widely distributed on the surface of the coastal plain (Fig. 3, *b*). The polygons have a tetragonal shape, most often square or rectangular. The diameter of the polygons is 12–15 m, less often up to 20 m, and increases to 50–60 m near the coastline on low-lying young terraces. All this indicates different ages and conditions of polygonal patterns formation in the lower reaches of the Yuzhnaya River. Almost all the polygons are divided into smaller ones by cracks of a higher generation. Near erosional downcuts filled with sandy-loamy deposits the flat-centered polygons transform into the high-centered ones owing to intense slumping of their slopes, resembling thermokarst mounds. Their height reaches 2 m, their diameter reaches 8 m. The depth of thaw was 0.45–0.50 m at the time of the studies.

Two polygons were studied during the course of the work – a high-centered (Fig. 4, *a*) and a flat-centered one (Fig. 4, *b*).

During the GPR sounding of the *high-centered polygon* two perpendicular profiles oriented south to north and east to west were drawn through it. The interval between the sounding points was 0.1 m. A100 antennas were used for layer-by-layer analysis of the top part of the section (TPS), and A150 with a higher resolution was used for detailed research. The obtained GPR profiles with topography taken into consideration are shown in Fig. 5.

During processing the GPR section was dissected into several GPR complexes (GC) [*Vladov, Starovoytov, 2004*] differing from one another in structure.

Fig. 4. Maria Pronchishcheva Bay.

Polygons: *a* – high-centered, *b* – flat-centered. Photo by D.E. Edemskiy.

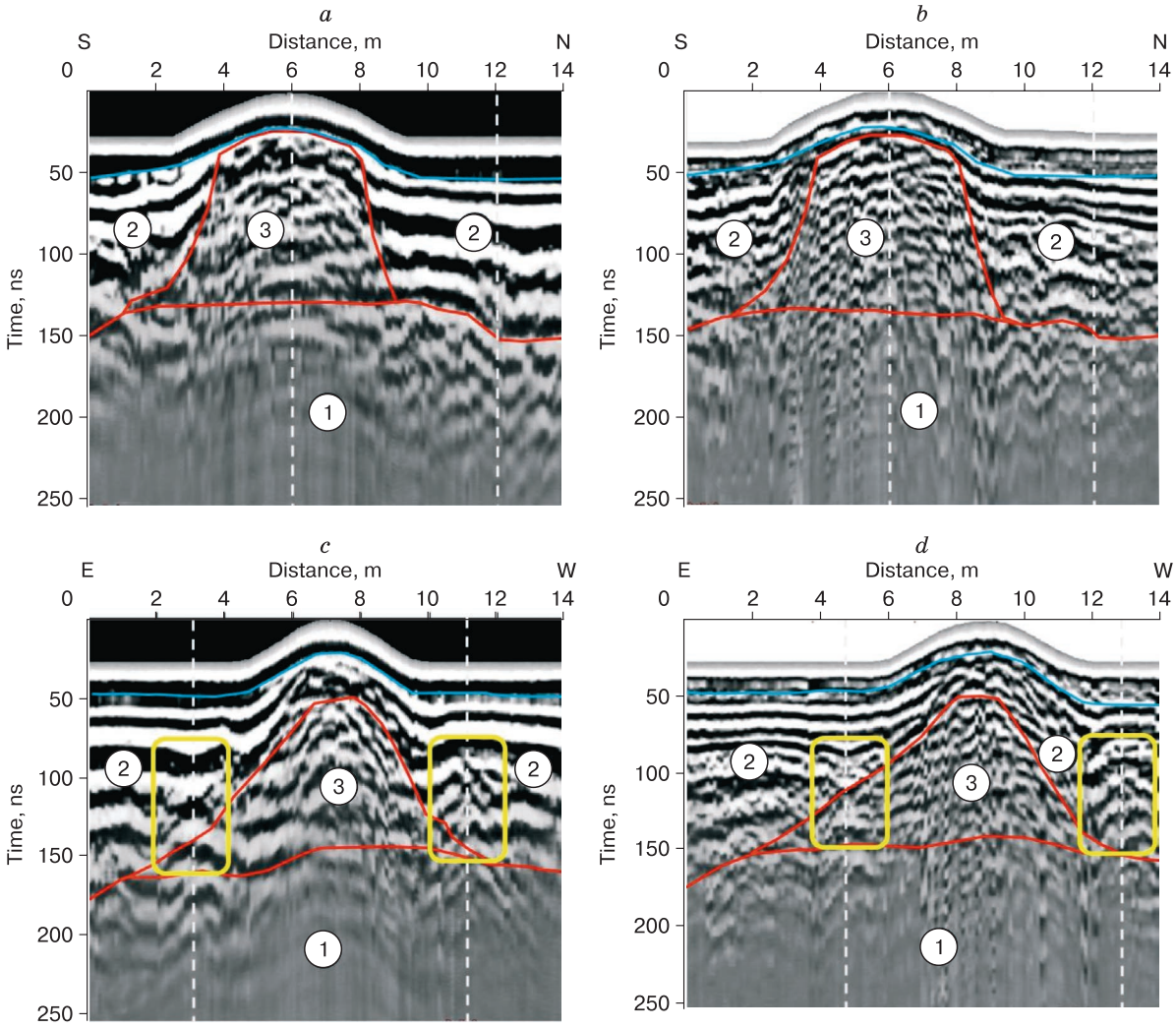

Fig. 5. Georadar profiles across a high-centered polygon.

a, *b* – meridional profile, A100 (*a*) and A150 (*b*) antennae; *c*, *d* – latitudinal profile, A100 (*c*) and A150 (*d*) antennas. 1–3 are the numbers of GPR complexes, the red lines show the boundaries between them, the blue line is the base of seasonally thawed layer. Heterogeneities are marked with yellow rectangles (see text).

The interfaces of the complexes are established based on intense reflecting horizons which match either layers of deposits of different composition or boundaries of unconformities.

The GPR complex GC1 is identified at the bottom of the studied part of the section, its top is located approximately at the 150 ns marks (4.5–5.5 m). GC3 matches the central part of the high-centered polygon (ground column) composed of sand-gravel deposits. A significant disturbance in phase axes before the 100–120 ns marks or approximately to depths of 3.0–4.4 m at an average electromagnetic wave velocity of 6.0–7.4 cm/ns is typical for GC3 (Table 1). GC2 matches troughs between the polygons. Its upper part (1.5–2.0 m thick) has a fairly clear parallel stratification along the whole length of the profile. On the slopes of the high-centered polygon, near the contact point with GC3, it is significantly deformed and inclined with a shift in the spatial position of in phase axes, local change in the re-

Table 1. **Results of processing of data collected using the common depth point method (M. Pronchishcheva Bay)**

Layer	Time, ns	Layer bottom depth, m	Average velocity, cm/ns	Thickness, m	Velocity, cm/ns	Relative dielectric permittivity
1	22.7	0.54	4.78	0.54	4.78	53.91
2	72.2	2.71	7.50	2.17	8.80	11.62
3	91.2	4.44	9.74	1.73	18.2	2.72
4	116.2	6.08	10.48	1.64	13.2	5.17

flected waves and a damping of their amplitude. The geological section GC2 is represented by peat and peaty sands.

Figure 5, *c* shows that in the lower parts of GC3 on the eastern and western sides (3 and 11 m marks), local heterogeneities are seen with peaks at 75–80 ns, identified on the image using yellow rectangles. The heterogeneity on mark 11 presents as semi-parallel inclined reflections which match the heterogeneity of the vertical ice wedge [*Elkarmoty et al., 2017*]. Near the 5 m mark (Fig. 5, *d*), beginning at 75 ns, a V-shaped structure is formed with corresponding curves of in phase axes of lower layers to the 120 ns mark, which can be interpreted as an ice-wedge pseudomorph.

During sounding of a polygonal patterns the primary reflection hyperbola which forms from the top of the wedge-shaped ice wedge, as well as the reflection from the bottom of the active layer, are usually difficult to distinguish on radargrams [*De Pascale et al., 2007; Munroe et al., 2007*]. This is related to their location at a small depth, where these signals are masked by the sounding impulse, air signals and are warped by reflections from near-surface layers and tears between blocks of the sod layer on the surface of the polygons.

Waveform spectrums obtained using the A100 antenna for the 6 m and 12 m marks (Fig. 5, *a*, *b*) are shown on Fig. 6, *a*, *b*. The amplitudes of the spectrum components for mark 6 in the center of the high-centered polygon are 25 % lower than the amplitudes for the 12 m mark, presumably owing to a disturbance of the surface layer by tears in sod. A change in the frequency of the spectrum of the received signal, seen in the appearance of two resonances at 85 and 102 MHz, should also be noted, which, together with the pattern of the reflected signal, can be interpreted as a result of a disturbance of the plane-layered media and the formation of randomly located reflection planes of distinct sizes.

During sounding of the *flat-centered polygon* similar GPR complexes were identified, but such significant changes are not seen in the reflection waveform. The subhorizontal structure in the near-surface layer GC2 is not disrupted overall up to 70–80 ns (Fig. 7). Nonetheless, changes are seen in both the near-surface layer (1.5–2.0 m thick) and in lower layers of sand-pebble deposits (GC1). There is no significant decrease in the signal level in the central part of the polygon at the 7 m mark also when analyzing the spectrum of the signal waveform (Fig. 8). The range of the high-frequency part of the spectrum for the central part of the polygon is limited by 80 MHz (Fig. 8, *a*) and 130 MHz (Fig. 8, *b*), while for the 12 m mark it is 130 MHz and 220 MHz, respectively. Apparently, this is result of structural changes in the upper layers (up to the mark near 65 ns) of the central part of the flat-centered polygon (GC3).

To determine the speed of electromagnetic wave propagation in the media and estimate the depth of GPR boundary location we used the CDP method with an interval of 0.1 m with a mutual relative antennas movement of a distance from 0.2 m to 6.0 m (Fig. 9). The GPR profile is drawn out three meters east of the high-centered polygon. The average electromagnetic wave propagation velocity has a general tendency to increase with depth from 4.78 cm/ns to 10.48 cm/ns and a respective change in dielectric permittivity from 53.91 to 2.72 (Table 1).

The obtained velocity propagation model consists of four layers. The top layer, up to 0.54 m thick and with an electromagnetic wave propagation velocity within the layer of v = 4.78 cm/ns, presents an active layer, while the lower layers present as layers of deposits of different granulometric compositions and, possibly, ice content, having electromagnetic wave propagation velocities in an interval of 8.8–18.2 cm/ns.

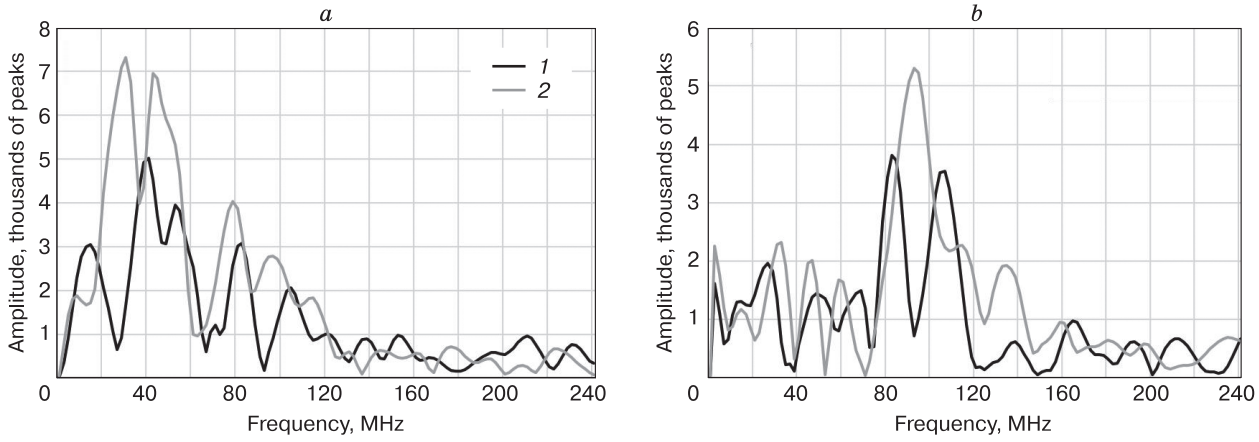

Fig. 6. Waveform spectrums for a high-centered polygon.

a – A100 antenna; *b* – A150 antenna; *1* – 6 m mark; *2* – 12 m mark. Position of marks see in Fig. 5, *a*, *b*.

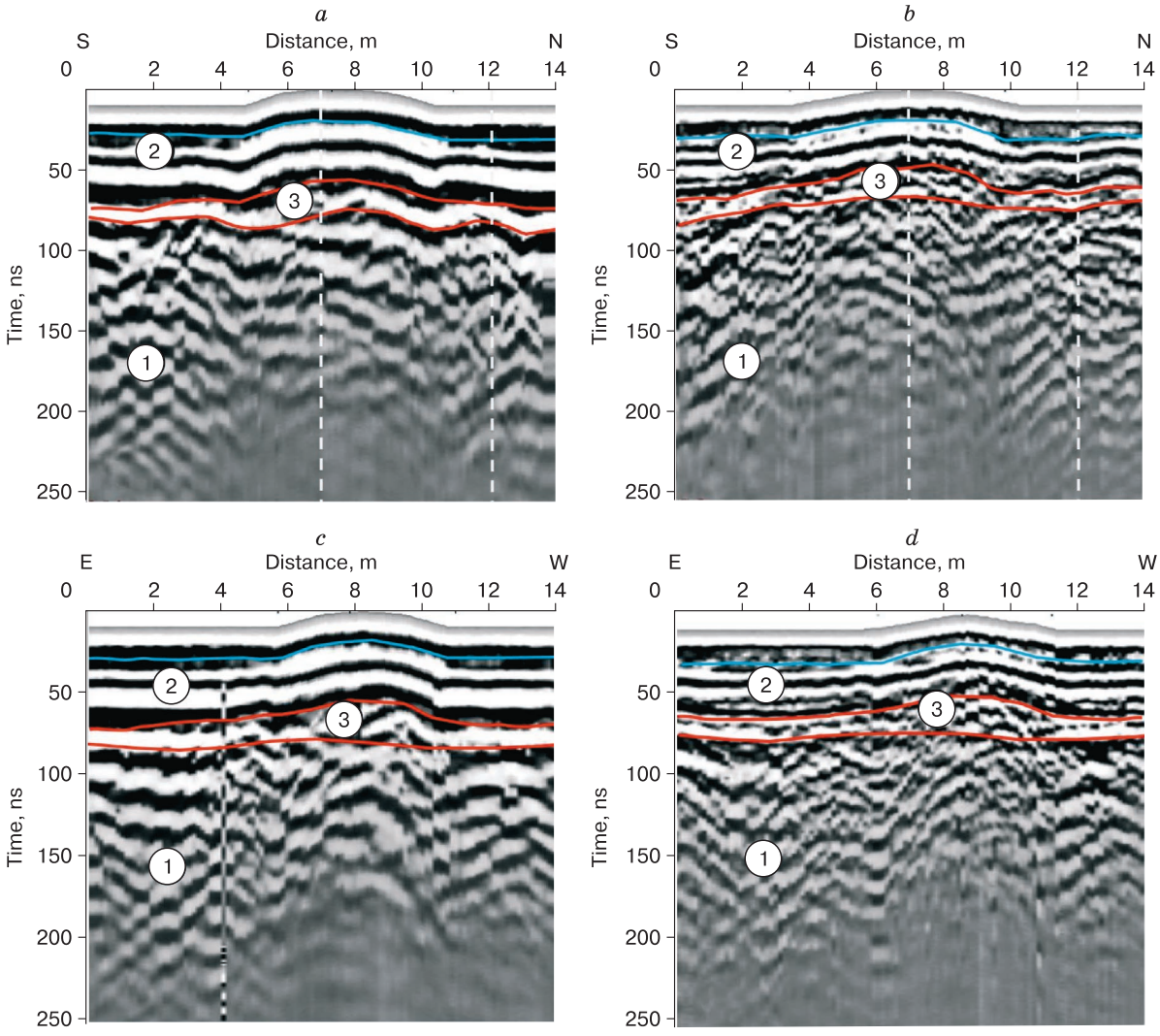

Fig. 7. Georadar profiles across a flat-centered polygon.

a, *b* – meridional profile, A100 (*a*) and A150 (*b*) antennas; *c*, *d* – latitudinal profile, A100 (*c*) and A150 (*d*) antennas. For other symbols see Fig. 5.

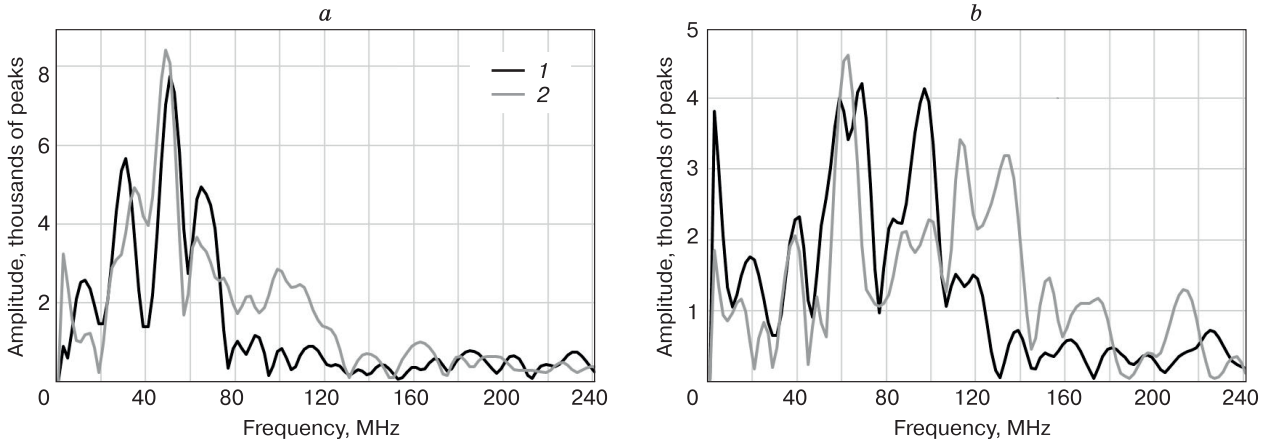

Fig. 8. Waveform spectrums for a flat-centered polygon.

a – A100 antenna; *b* – A150 antenna; *1* – 7 m mark; *2* – 12 m mark. Position of marks see in Fig. 7, *a*, *b*.

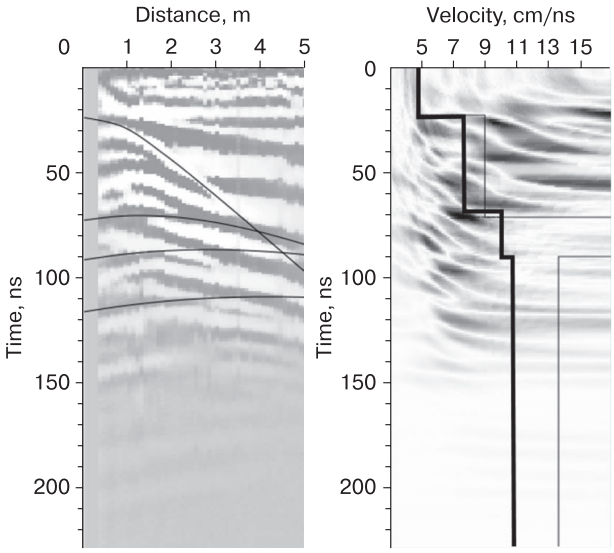

Fig. 9. The results of determining the speed of electromagnetic wave propagation (M. Pronchishcheva Bay).

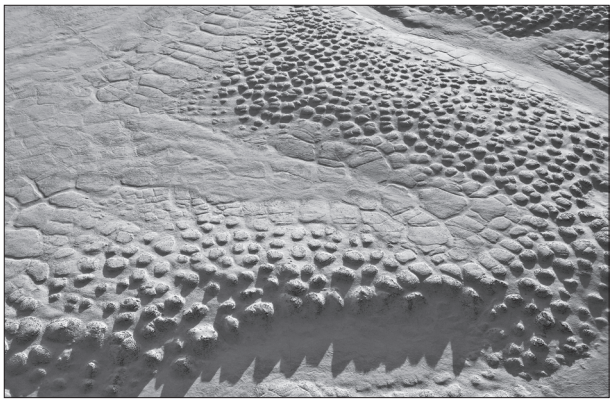

Fig. 10. Polygonal patterns in the research area southwest of Cape Walter, near the Nerpalakh Lagoon (Kotelny Island).

Photo by R.A. Zhostkov.

Kotelny Island, Nerpalakh Laguna area

The second research area is located on the sea coast southwest of Nerpalakh Laguna (75°22′4.61″ N, 137°5′19.29″ E). Here the coast forms a sheer cliff up to 25 m high in which layers of lithified Paleozoic carbonate-terrigenic sedimentary rocks are exposed. The surface of the high part of the coast is dissected by multiple hollows. Between and throughout them, a degrading polygonal network which forms low- and intermediate-centered polygons about 15–20 m large is distributed (Fig. 10). Morphologically they are in many ways similar to the polygons near M. Pronchishcheva Bay. The central part of the polygons is in many cases represented by flat-topped mounds up to 2 m high and up to 10 m in diameter. The vegetation is represented by moss and lichen, and by grasses at the tops and forms a thick sod cover which is ripped into separate blocks in most instances (Fig. 11).

In this site, the key point for the analysis of the structure is the depth of rock base. The rocks are represented by alternating layers of black carbonized schists, siltstone, fine grain sandstones and limestones which all have a dip of 45° with a inclination toward the northeast. At their top, in the bottom of disperse deposits cover, an eluvial horizon of varying thickness represented by debris of varied grain sizes is located.

As in the vicinity of M. Pronchishcheva Bay, two types of polygons can be identified here: high-centered polygons up to 2.0–2.5 m in height (Fig. 11, *a*) and flat-centered polygons up to 1 m high (Fig. 11, *b*). They are all 4 to 8 m in diameter and are located on a gentle slope descending towards the sea. The depth of thaw during the survey was 0.40–0.45 m.

A GPR profile through a high-centered polygon about 2 m high and 6 m in diameter is presented in Fig. 12. Its surface is covered with separate sod hummocks, predominantly round, with a diameter of 30–40 cm and no taller than 10–15 cm. The measurements were obtained using an A150 antenna with the 15-cm interval along the profile.

Rock base GC1 is identified in the bottom of the GPR section. Its geological structure was studied in the coastal ledge up to 20 m high, located at a 150 m distance from the profile. The upper part of the GPR section (GC2), represented by peaty loamy sand deposits, has a rather clear subhorizontal stratification. It is most likely linked to the cover layer of disperse deposits 1.5–2.0 m thick. Between GC1 and GC2, the GC3 is identified based on different nature of the signal. We associate it with a layer of disperse deposits and products of rock base destruction, in other words, eluvium (GC3) up to 1 m thick.

Homogenous deposits are seen in the GPR profile in GC1 and GC2, and no signs of ice wedges or pseudomorphs are registered. The lower part of the GPR profile of the high-centered polygon in is identified as an area with a low electromagnetic wave amplitude and a blurred wave patterns (area 4 on Fig. 12). Signal attenuation is apparently caused by scattering of the sounding signal in disperse deposits of GC3, which form the central part of the polygon.

The wave spectrum for the central part of the polygon (mark 11) has a smoother shape compared to the 4 m mark (Fig. 13). Additionally, the formation of a main spectral maximum at a frequency of 78 MHz and two with a lower amplitude at frequencies of 46 and 115 MHz are typical for it. This can be interpreted as a result of changes in the layered structure of disperse deposits cover (GC3) with a formation of

Fig. 11. Kotelny Island.

Polygons: *a* – high-centered, *b* – flat-centered. Photo by D.E. Edemskiy.

contrasting boundaries which contribute to the formation of spectral maxima at these frequencies.

The width of the signal spectrum at the 0.5 level of its maximum amplitude (mark 11) is more than two times less than that of mark 4 m, where frequencies from 90 to 170 MHz prevail. This may be related to weakening of the sounding signal in GC2 and GC3 and a smaller contribution of signals reflected from heterogeneities in the rock base to the resulting spectrum (GC1).

A GPR profile drawn through two high-centered polygons 0.8 and 1.2 m high, 4 and 6 m in diameter, respectively, is presented in Fig. 14. The polygons are located on a gentle northeastern slope of the upland. As in the previous example, GC1 composes a rock base with an eluvial horizon on top (GC3). The upper part of GPR section GC2 has a fairly clear subhorizontal layering.

Signals are registered in Fig. 14 within GC3 (radiolocational images of local objects) which may be large fragments of underlying bedrock. The presence of these heterogeneities leads to additional signal attenuation, as a result of which areas with lower wave amplitude (area 4 on Fig. 14) and significant weakening of equiphase lines in GC1 form on the profile. The area of signal attenuation captures not the entire area of the polygon, but only a part of it, under local heterogeneities.

Among the spectra demonstrated in Fig. 15 it can be seen that the main maxima for two marks

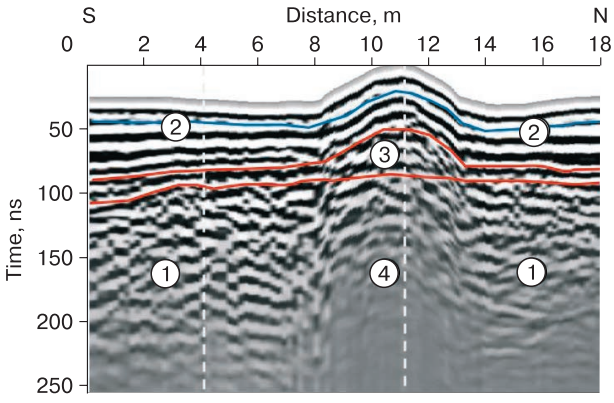

Fig. 12. Georadar profile across a high-centered polygon, A150 antenna.

1–3 – numbers of GPR complexes, 4 – area of signal attenuation. The red lines show the boundaries between the GPR complexes, the blue line is the bottom of the seasonally thawed layer, the white dashed lines are the marks for which the spectral analysis was carried out.

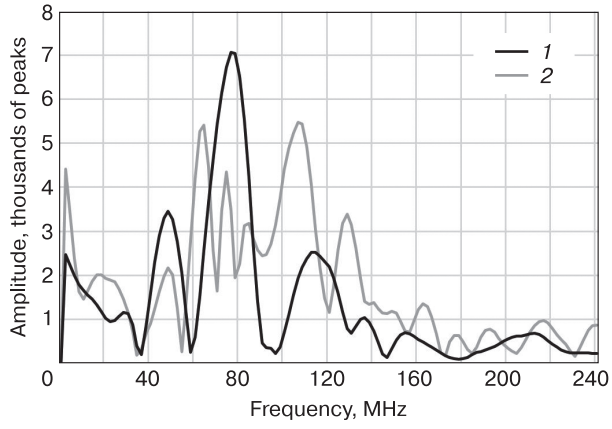

Fig. 13. Waveform spectrums for a high-centered polygon, A150 antenna.

1 – 4 m mark; *2* – 11 m mark. Position of marks see in Fig. 12.

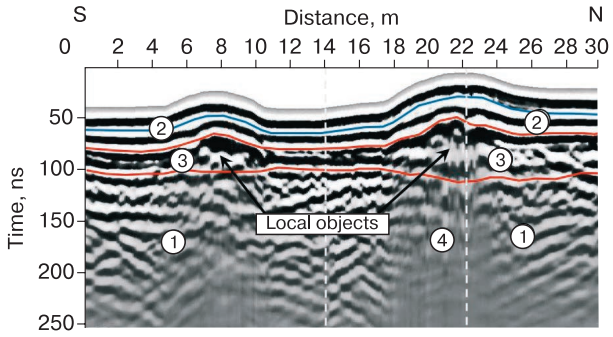

Fig. 14. Georadar profile across two high-centered polygons, A100 antenna.

For symbols see Fig. 12.

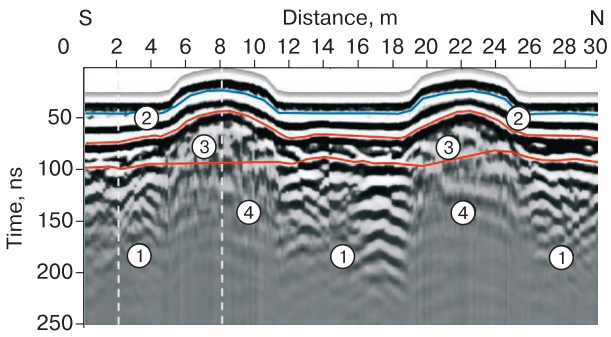

Fig. 16. Georadar profile across two flat-centered polygons, A100 antenna.

For symbols see Fig. 12.

(14 m and 22 m) are located at 60 MHz, however, the amplitude of the spectral component is 38 % lower for the central part of the polygon than for the 14 m mark, which is supposedly caused by structural peculiarities of GC3, positioned between the bottom of the subhorizontal sedimentary deposits and the top of the bedrock. Damping of the amplitude of the spectral component and the formation of a smoother spectrum shape may indicate a propagation process of the signal in GC3, which can also be interpreted as a change in the structure of the top layers of the section and the appearance of new boundaries or interlayers up to approximately 100 ns marks in the central part of the high-centered polygon [*Schennen et al., 2016*].

Further down the slope, towards the coast, the relative height of the polygons decreases to 1 m, and their surface becomes more flat and less destroyed. Figure 16 shows a GPR profile drawn through two flat-sentered polygons 7 and 8 m in diameter and 1.0–1.1 m high.

Overall, the GPR profile structure is identical to the previous ones (Figs. 12, 14). The thickness of the active layer is 0.40–0.45 m (measured by a dipstick), the water content of the deposits in the active layer is uneven. The top horizon of disperse deposits (GC2) forms a specific structure with parallel subhorizontal stratification, the thickness of which is comparable to the analogous GC on Fig. 12 and 14. The bottom of GC2 in the body of the flat-centered polygon is located at the 50–65 ns mark (1.5–2.0 m at an average electromagnetic wave velocity of 6 cm/ns). The body of the polygon is identified on the profile as an area with significant amplitude attenuation of the sounding signal (GC4) and, as a result, an absence of in phase components in lower layers of the profile.

In the spectral region (Fig. 17) the left polygon differs from the previously discussed one in its shift into the low-frequency region of the spectrum maximum for a 50 MHz interpolygonal trough, which is possibly related to the bedrock structure of the GC1.

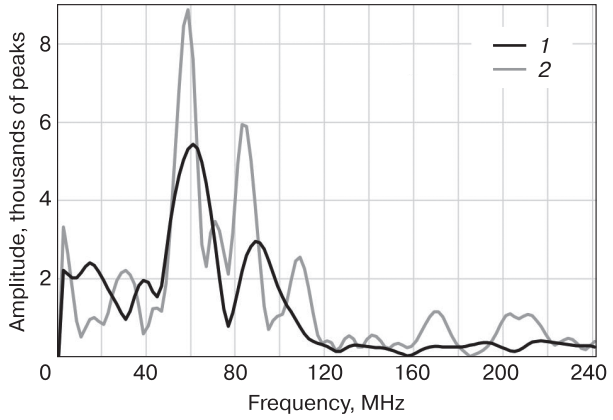

Fig. 15. Waveform spectrums for a high-centered polygon, A100 antenna.

1 – 14 m mark; *2* – 22 m mark. Position of marks see in Fig. 14.

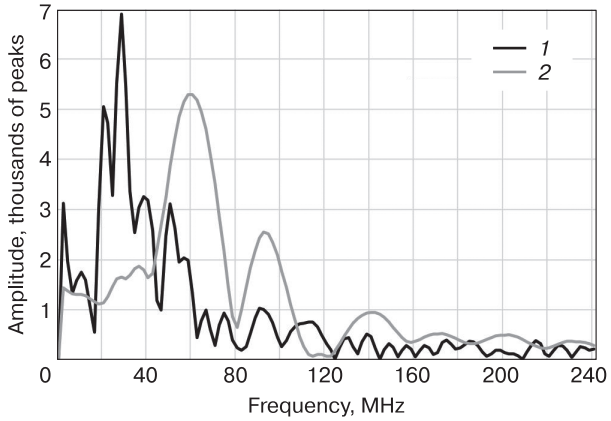

Fig. 17. Waveform spectrums for a flat-centered polygon, A100 antenna.

1 – 2 m mark; *2* – 8 m mark. Position of marks see in Fig. 16.

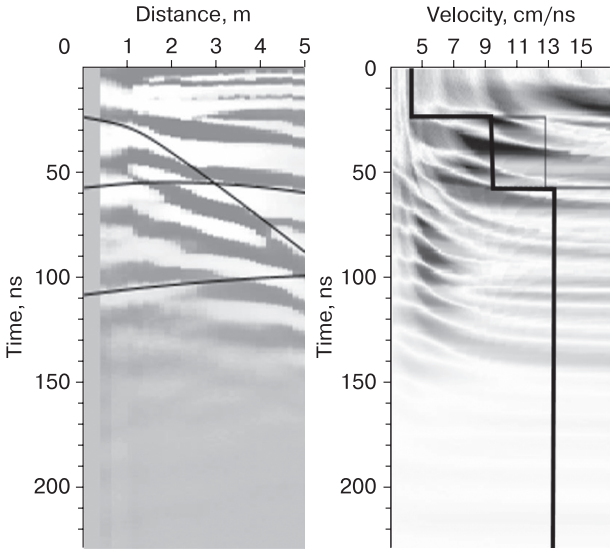

Fig. 18. The results of determining the speed of electromagnetic wave propagation (Kotelny Island).

The spectrum for the central part of the polygon (8 m mark) is almost identical in its parameters (central frequency, amplitude) to the spectrum for the polygon in Fig. 14. The smoothed shape of the signal spectrum and almost total absence of signals from the bedrock (GC1) may indicate only a scatter process in GC3, between the bottom of the disperse deposits horizon and the top of the bedrock. The nature of the changes and the reasons leading to them require additional research and interpretation.

To determine the velocity of the sounding impulse propagation and to estimate the depths of separate layers of the section, studies were completed using the CDP method with an interval of 0.1 m and a distance from 0.2 m to 4.6 m between antennae (Fig. 18). The CDP profile is located in close proximity to the high-centered polygon. According to sounding data, electromagnetic wave propagation velocity increases with depth from 4.26 cm/ns to 12.83 cm/ns, and dielectric permittivity increases from 49.76 to 3.11 (Table 2).

Table 2. **Results of processing of data collected using the common depth point method (Kotelny Island)**

Layer	Time, ns	Layer bottom depth, m	Average velocity, cm/ns	Thickness, m	Velocity, cm/ns	Relative dielectric permittivity
1	23.6	0.50	4.26	0.50	4.26	49.76
2	58.1	2.65	9.14	2.15	12.4	5.85
3	109.8	7.06	12.83	4.41	17.0	3.11

The obtained model of propagation velocity consists of three layers. The top layer up to the 23.6 ns mark and with an electromagnetic wave propagation velocity of 4.26 cm/ns presents an active layer 0.5 m thick. The lower layers are deposits of different granulometric composition and, possibly, ice content, having a wave propagation velocity in the range of 9.14–12.83 cm/ns.

DISCUSSION

All the studied polygons, both in Maria Pronchishcheva Bay and on the western coast of Kotelny Island, were formed during a process of long-term frost cracking and the formation of ice wedges. Similarity in the deposits in which they formed is typical for them: in all cases they were developed in relatively coarse deposits represented by sands and sands

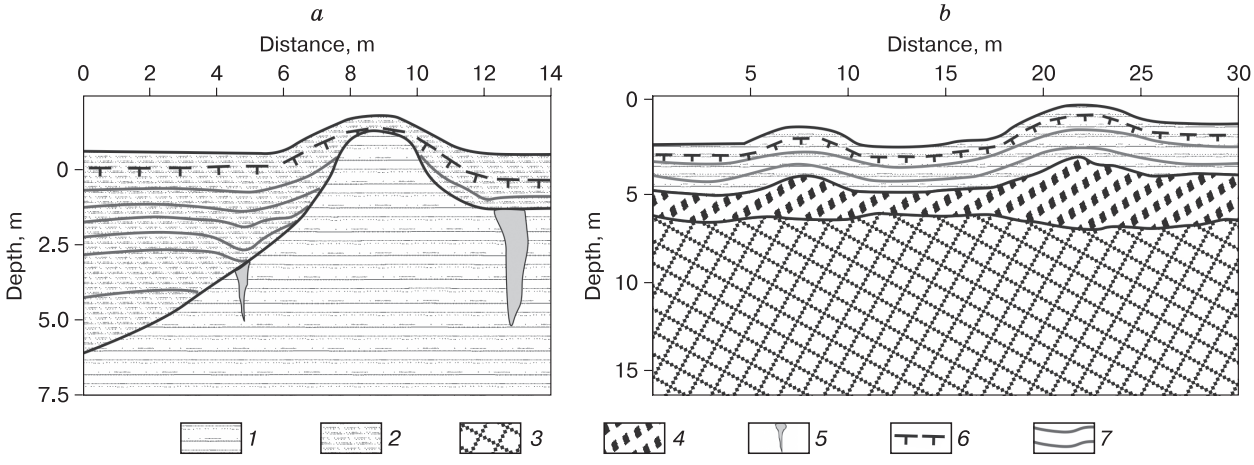

Fig. 19. Geological sections built based on the interpretation of typical GPR profiles.

a – the profile across the high-centered polygon in the M. Pronchishcheva Bay (see Fig. 5, *d*); *b* – the profile across two high-centered polygons at Kotelny Island (see Fig. 14). *1* – sand and gravel deposits; *2* – sandy and sandy loamy deposits, varying in peat amount; *3* – bedrock; *4* – eluvium with fragments of bedrock; *5* – ice wedges; *6* – seasonally thawed layer base; *7* – layering in disperse deposits.

with gravel, overlapped by peaty deposits or peat. Currently the polygonal pattern is in a stage of degradation in both regions: the ice wedges are partially or totally thawed, depressions have formed above them and ground columns have transformed into high or flat-topped mounds. Owing to solifluction processes on their slopes, these mounds gradually decrease in diameter and height, the width of the troughs between them increases. Thawed material moves into the troughs between the mounds and then slowly travels down the slope, forming a thin cover of deluvial-solifluctional deposits with parallel layering in troughs above what was previously ice wedges. The supposed geological sections of the deposits constructed from the results of GPR studies of two typical profiles are shown in Fig. 19.

GPR studies did not show a presence of ice wedges in depressions, with the exception of one area near a high-centered polygon in M. Pronchishcheva Bay (Fig. 5). Ice wedges either melted completely or were preserved as a thin lower part which does not get registered by the GPR. Deluvial-solifluctional deposits lie more or less parallel to the surface. At their base, structures resemblant of pseudomorphs are found only in M. Pronchishcheva Bay. Most likely, the ice wedges on Kotelny Island penetrated into relatively coarse bedrock eluvium, which does not cause significant subsidence when thawing.

In all cases the inner structure of the polygons showed the presence of heterogeneities most likely related to ground ice content distribution. For GPR profiles in M. Pronchishcheva Bay weak signal attenuation and general conformity of the radargram to the topography are typical: within the more high-centered mound a larger rise in in-phase lines is seen compared to the flat-centered polygon. On Kotelny Island the situation is similar, but here the peculiarities of the structure of the eluvial horizon on the boundary of bedrock and disperse deposits apparently play an important role.

RESULTS

Georadiolocational research of a polygonal pattern at the degradation stage, which exists in modern severe permafrost conditions, was conducted on the eastern coast of Taymyr Peninsula and on the western coast of Kotelny Island. As a result of thawing of the polygonal surface, the ground columns are represented by slightly high-centered or flat-centered forms. They are composed predominantly of sandy material.

The results of the studies allowed us to see the inner structure of the high-centered polygon, its boundaries, to establish an almost total degradation of ice wedges and the possible presence of pseudomorphs in the M. Pronchishcheva Bay area. A poor expression of the pseudomorphs is attributed to the deposit composition (frost-stable sands) and the close proximity of the bedrock on Kotelny Island.

In the present work a method based on joint frequency-time analysis of GPR data was used for a more precise qualitative estimate of changes occurring in the geological media. It was shown that the peak part of the spectrum is unique in different conditions and for different structural changes in frozen ground horizons, which indicates an ability of spectral analysis for the differentiation of heterogeneities under the polygonal patterns.

According to sounding data based on the CDP method, the electromagnetic wave propagation velocity in the section increases with depth from 4.26 cm/ns to 18.2 cm/ns, and dielectric permittivity changes within the range from 53.91 to 2.72.

Overall, the conducted GPR sounding of several polygons in similar geocryological conditions raised more questions than provided answers.

GPR should be considered among the main tools for permafrost studies. Compared to other geological and geophysical methods, GPR allows to determine in detail the inner structure of an object, the shape of geological boundaries, the structure of a section. Further field work in areas with different permafrost structure and polygonal patterns is necessary for verification of the results of GPR sounding.

Acknowledgments. *The authors thank the Russian Geographical Society for assistance in the organization and completion of this research.*

References

Anbazhagan, P., Chandran, D., Burman, S., 2014. Subsurface imaging and interpretation using Ground Penetrating Radar (GPR) and Fast Fourier Transformation (FFT). Advances in Soil Mechanics and Geotechnical Engineering, vol. 3, 254–259.

Benedetto, F., Tosti, F., 2013. GPR spectral analysis for clay content evaluation by the frequency shift method. J. Appl. Geophys., No. 97, 89–96.

Buzin, V., Edemskiy, D., Gudoshnikov, S., et al., 2017. Search for Chelyabinsk meteorite fragments in Chebarkul Lake bottom (GPR and Magnetic Data). J. Telecommun. and Information Technol., No. 21, 69–78.

De Pascale, G.P., Pollard, W.H., Williams, K.K., 2007. Geophysical mapping of ground ice using a combination of capacitive coupled resistivity and ground-penetrating radar, Northwest Territories, Canada. J. Geophys. Res. 113 (2), F02S90.

Dostovalov, B.N., 1952. On the physical conditions for the formation of frost cracks and the development of fissured ice in disperse rocks. Issledovaniya vechnoy merzloty v Yakutskoy respublike [Permafrost Investigations in Republic of Yakutia], iss. 3, 162–194 (in Russian).

Edemskiy, D.E., Edemskiy, F.D., Morozov, P.A., 2010. Profiling and determination of media parameters during GPR surveys. Elektromagnitnye volny i elektronnye sistemy [Electromagnetic Waves and Electronic Systems], 15 (9), 57–63 (in Russian).

Edemskiy, D.E., Popov, A.V., Prokopovich, I.V., et al., 2018. Ground penetrating radars application for soil-pyroclastic cover survey of the south-eastern zone of Matua Island, the

Kurile Islands. Vestnik Kamchatskoy regional'noy assotsiatsii "Uchebno-nauchnyy tsentr". Seriya: Nauki o Zemle [Bulletin of Kamchatka Regional Association "Educational-Scientific Center". Earth Sciences], iss. 40 (4), 69–81 (in Russian).

Edemskiy, D.E., Popov, A.V., Prokopovich, I.V., et al., 2019. Application of geophysical methods in the survey of the periphery of the Tunnug-1 mound. Intern. J. Appl. and Basic Res., No. 11, 40–48.

Elkarmoty, M., Colla, C., Gabrielli, E., et al., 2017. Mapping and modelling fractures using ground-penetrating radar for ornamental stone assessment and recovery optimization: Two case studies. The Mining-Geology-Petroleum Engineering Bulletin, 32 (4), 63–76.

Finkelstein, M.I., Kutev, V.A., Zolotarev, V.P., 1986. Application of Radar Subsurface Sounding in Engineering Geology. Nedra, Moscow, 128 pp. (in Russian).

Kaplina, T.N., Romanovskii, N.N., 1960. About ice-wedge casts. In: Periglacial Forms on the USSR Territory. Moscow, pp. 47–59 (in Russian).

Kopeikin, V.V., Edemskiy, D.E., Garbatsevich, V.A., et al., 1996. Enhanced power ground penetrating radars. In: Proc. of the 14th Intern. Conference on Ground Penetrating Radar, Sendai, Japan, pp. 152–154.

Kopeikin, V.V., Morozov, P.A., Edemskiy, F.D., Edemskiy, D.E., et al., 2012. Experience of GPR application in oil-and-gas industry. In: Proc. of the 14th International Conference on Ground Penetrating Radar, Shanghai, China, vol. 3, pp. 817–819.

Léger, E., Dafflon, B., Soom, F., et al., 2017. Quantification of Arctic soil and permafrost properties using ground-penetrating radar and electrical resistivity tomography datasets. In: IEEE J. Selected Topics in Appl. Earth Observations and Remote Sens., No. 10, 4348–4359.

Munroe, J.S., Doolittle, J.A., Kanevskiy, M.Z., et al., 2007. Application of ground-penetrating radar imagery for three-dimensional visualization of near-surface structures in ice-rich permafrost, Barrow, Alaska. Permafrost and Periglacial Processes 18, 309–321.

Neradovskii, L.G., Fedorova, L.L., 2020. Experience in studying the nature of the periodicity of GPR signals using spectral analysis methods. Uspekhi sovremennogo estestvoznaniya [Advances in Modern Natural Science], No. 6, 95–106 (in Russian).

OOO "VNIISMI Company" [Web]. – URL: http://www.georadar.ru/ (last visited: 05.03.2021) (Russian and English).

Romanovskii, N.N., 1977. Formation of Polygonal-wedge Structures. Nauka, Novosibirsk, 1977, 213 pp. (in Russian).

Schennen, S., Tronicke, J., Wetterich, S., et al., 2016. 3D ground-penetrating radar imaging of ice complex deposits in northern East Siberia. Geophysics 81 (1), wa185–wa192.

Sudakova, M.S., Sadurtdinov, M.R., Malkova, G.V., Skvortsov, A.G., Tsarev, A.M., 2017. Ground penetrating radar applications to permafrost investigations. Earth's Cryosphere XXI (3), 62–74.

Vladov, M.L., Starovoytov, A.V., 2004. Introduction to Ground Penetrating Radar. Izd-vo MGU, Moscow, 2004, 153 pp. (in Russian).

Voronin, A.Ya., 2015. Criteria for identifying the structure and functional properties of the soil profile in GPR studies using the "LOZA-V" GPR. In: Byulleten Pochvennogo instituta im. V.V. Dokuchaeva [Dokuchaev Soil Bulletin], No. 80, pp. 106–128 (in Russian).

YongShuai, Y., Yajing, Y., Guizhang, Z., 2019. Estimation of sand water content using GPR combined time-frequency analysis in the Ordos Basin, China. Open Physics 17, 999–1007.

Received March 29, 2021
Revised April 15, 2021
Accepted June 1, 2021

Translated by M.A. Korkka